Chemosphere 138 (2015) 758–764

Contents lists available at ScienceDirect

Chemosphere

journal homepage: www.elsevier.com/locate/chemosphere

Kinetic modeling of pH-dependent antimony (V) sorption and transport in iron oxide-coated sand

Yongbing Cai [a,b], Lulu Li [c], Hua Zhang [a,*]

[a] Key Laboratory of Coastal Zone Environmental Processes and Ecological Remediation, Yantai Institute of Coastal Zone Research, Chinese Academy of Sciences, Yantai, Shandong, China
[b] University of Chinese Academy of Sciences, Beijing, China
[c] College of Chemical and Environmental Engineering, Qingdao University, Qingdao, Shandong, China

HIGHLIGHTS

- Decreased Sb(V) sorption capacity and kinetic rate under alkaline condition.
- Inner-sphere surface complexation of Sb(V) on iron oxide coated sand.
- Increased mobility of Sb(V) caused by deprotonation on oxide surface.
- Nonlinear MRM model well describes time-dependent retention and transport.

ARTICLE INFO

Article history:
Received 25 February 2015
Received in revised form 23 July 2015
Accepted 25 July 2015
Available online 18 August 2015

Keywords:
Antimony
Iron oxide-coated sand
Adsorption–desorption
Transport

ABSTRACT

Understanding the mechanisms and kinetics controlling the retention and transport of antimony (Sb) is prerequisite for evaluating the risk of groundwater contamination by the toxic element. In this study, kinetic batch and saturated miscible displacement experiments were performed to investigate effects of protonation–deprotonation reactions on sorption–desorption and transport of Sb(V) in iron oxide-coated sand (IOCS). Results clearly demonstrated that Sb(V) sorption was highly nonlinear and time dependent, where both sorption capacity and kinetic rates decreased with increasing solution pH. Breakthrough curves (BTCs) obtained at different solution pH exhibited that mobility of Sb(V) were higher under neutral to alkaline condition than under acidic condition. Because of the nonlinear and non-equilibrium nature of Sb(V) retention and transport, multi-reaction models (MRM) with equilibrium and kinetic sorption expressions were utilized successfully to simulate the experiment data. Equilibrium distribution coefficient (K_e) and reversible kinetic retention parameters (k_1 and k_2) of both kinetic sorption and transport experiment showed marked decrease as pH increased from 4.0 to 7.5. Surface complexation is suggested as the dominant mechanism for the observed pH-dependent phenomena, which need to be incorporated into the kinetic models to accurately simulate the reactive transport of Sb(V) in vadose zone and aquifers.

1. Introduction

Antimony (Sb) and its compounds are considered as toxic or carcinogenic to human health (Gebel et al., 1997; Beyersmann and Hartwig, 2008). In general, the natural abundance of Sb is low, 0.2–2 $\mu g\, g^{-1}$ in sediment rocks, <1 $\mu g\, L^{-1}$ in natural water, and few $\mu g\, g^{-1}$ in sediments and soils (Filella et al., 2002a). Elevated Sb concentrations are found in soil and water around mining and smelting sites, at shooting ranges, and along roadsides (Scheinost et al., 2006; Wilson et al., 2010; He et al., 2012). For instance, China has suffered serious Sb pollution in several regions where Sb concentrations in soils were up to thousand times higher than natural background (He et al., 2012). Although field and laboratory experiments have been carried out to investigate the environmental behaviors of Sb, there are still substantial knowledge gaps on the fate and transport of Sb in soil and aquifer. Specifically, the lack of appropriate model and model parameterization has limited our ability to evaluate the environmental and ecological risks of Sb contamination.

Sb is mostly present in the form of oxyanions, primarily in trivalent (III) or pentavalent (V) state in soil solution and aqueous environments. Antimonate [Sb(V)] is the predominant and thermodynamically stable Sb species in oxic and suboxic

* Corresponding author.
E-mail address: hzhang@yic.ac.cn (H. Zhang).

http://dx.doi.org/10.1016/j.chemosphere.2015.07.067
0045-6535/

environment (Takayanagi and Cossa, 1997; Leuz and Johnson, 2005; Ilgen et al., 2014) and antimonite [Sb(III)] predominates under reducing conditions (Hockmann et al., 2014). Based on the hydrolysis reaction of antimonic acid [$Sb(OH)_5 + H_2O \leftrightarrow Sb(OH)_6^- + H^+$, $pK_1 = 2.85$], the hydroxyanion $Sb(OH)_6^-$ species predominates at environmental pH values (Accornero et al., 2008). Earlier studies have indicated soil properties including metal content, organic matter, pH and redox conditions as potential controlling factors of Sb retention and transport in soils (Frohne et al., 2011). Leuz et al. (2006) found that both Sb(III) and Sb(V) bind strongly to hydroxides of Fe, Al, and Mn and only weakly to clay minerals. Sb(V) sorption on Fe hydroxides maximizes at low pH and decreases after pH 7. It has been reported that 95% Sb(V) sorption by a non-crystalline Fe hydroxide across a pH range of 2.5–7 with a sorption maximum at about pH 4 (Tighe and Lockwood, 2007). Extended X-ray absorption fine structure (EXAFS) results concluded that Sb(V) formed monodentate-mononuclear and bidentate-binuclear inner-sphere surface complexes on Al and Fe oxides (Scheinost et al., 2006; Mitsunobu et al., 2010; Ilgen and Trainor, 2012; Ritchie et al., 2013; Guo et al., 2014). Surface complexation models (SCMs) have been used to simulate the adsorption of Sb(V) onto a wide range of adsorbents and are successful in predicting the effects of solution pH and ionic strength (Vithanage et al., 2013; Essington, 2013; Rakshit et al., 2015). However, most researches on Sb(V) sorption were equilibrium studies conducted in a relatively short duration (usually 24 h), which has limited value for predicting non-equilibrium or time dependent transport of Sb(V) in geological media (Martinez-Llado et al., 2011). Recently, Zhang et al. (2014) demonstrated that Sb (V) sorption capacity and kinetic rate of the acidic red soil was much higher than that of the calcareous soil and suggested that pH is a major environment variable responsible for the different sorption and transport behavior.

Although the effect of pH on Sb(V) sorption was already known (Tighe et al., 2005; Willis et al., 2011; Biver et al., 2011; Vithanage et al., 2013; Rakshit et al., 2015), little analysis had been conducted to investigate the mechanisms and kinetics controlling protona tion–deprotonation reaction effects on Sb(V) transport. In this study, the kinetic batch and column transport experiments were carried out to quantify the extent of pH effect on the reactive transport of Sb(V) in iron oxide-coated sand. The multi-reaction models (MRM) with equilibrium and kinetic formulations were evaluated for their capability to describe the pH-dependent sorption and transport of Sb(V). This study will provide essential information for evaluating the environmental risks associated with Sb release at contaminated sites.

2. Material and methods

2.1. Iron oxide-coated sand

Iron oxide-coated sand (IOCS) was prepared by mixing 87.5 mL of 0.17 M $Fe(NO_3)_3$ and 90.0 mL of 0.52 M NaOH with 500 g clean quartz sand in an evaporating dish. The mixture was placed in oven at 105 °C for 72 h and stirred periodically to prevent crusting of salts on surface. After coating the quartz sand with iron oxyhydroxide, the coated sand was washed sequentially in 1.0 mM HCl and 1.0 mM NaOH to remove weakly absorbed iron on the sand surface and followed by rinsing with ultrapure water until no change of color in solution. The synthesis procedure is same to that reported by Wang et al. (2011, 2012) who found that 75 ± 3% of the grain surfaces of the iron coated sand were coated by iron oxyhydroxide using SEM–EDX (Scanning Electron Microscopy–Energy Dispersive X-ray) analysis (SSX-550, Shimadzu).

2.2. Batch experiments

Equilibrium sorption isotherms and sorption edges were determined using batch experiments at room temperature (25 °C) under aerobic conditions (Zhang and Selim, 2005). Experiments were initiated by mixing 3.0 g of IOCS with 20 mL of 0.01 M $KClO_4$ background solution in 50-mL Teflon tubes and adjusting solution to desired pH at 3.0, 4.0, 6.0, 7.5 and 9.0 using Metrohm 888 Titrando automatic titrator (Metrohm, Switzerland). After the pH was stabilized, initial concentrations (C_0) of Sb(V) ranging from 8.3×10^{-3} to 2.5×10^{-1} mM were achieved by adding stock solution of $KSb(OH)_6$ followed by readjusting solution pH. Then the total volumes were brought to 30 mL with background solution. The mixtures were shaken at 150 rpm on a reciprocal shaker for 48 h and subsequently centrifuged for 10 min at 4000 rpm before sampling. A 1-mL aliquot was sampled from the supernatant and subsequently diluted to 10 mL for analysis.

To determine extent of time-dependent sorption and desorption, kinetic batch experiments were initiated with two initial concentrations C_0 (8.3 and 83 μM) of Sb(V). The mixtures were sampled at reaction times of 0.5, 2, 6, 12, 24, 48, 168, and 240 h after centrifuging. After each sampling, measure and adjust the slurry to its original pH before returning back to the shaker. Amount of Sb(V) sorption was calculated from the difference between concentrations of the supernatant and that of the initial solutions. Desorption of Sb(V) was quantified using the same batch system immediately after the last sorption step (240 h). Each desorption step was carried out by sampling and measuring the pH of the supernatant after centrifugation, and then replacing the supernatant with 30 mL 0.01 M $KClO_4$ background solution, and shaking for 24 h. This desorption step was iterated four times with a total desorption time of 96 h.

Concentrations of total Sb were analyzed using Hydride Generation Atomic Fluorescence Spectrometer (HG-AFS, AFS-930, Beijing jitian Instrument Factory Co., Ltd., Beijing). Amount of Sb (V) sorbed was calculated from the difference between concentrations of the supernatant and that of the initial solutions. The fraction of Sb(V) desorbed from the soils were calculated based on the change in concentration in solution (before and after desorption). The experiments were performed in triplicates and the mean and standard error (SE) of the amount of Sb(V) adsorbed is reported.

2.3. Miscible displacement experiments

The transport of Sb(V) in columns of IOCS was investigated using the saturated miscible displacement technique (Zhang and Selim, 2006, 2011). Acrylic columns (8.5-cm in length and of 2.5-cm internal diameter) were uniformly packed with IOCS and were slowly water saturated with background solution of 0.01 M $KClO_4$ with different pH (4.0, 6.0, and 7.5) at a low Darcy flux until desired pH values (4.0, 6.0, and 7.5) were reached in effluent. Input solution of 0.15 mM Sb(V) in 0.01 M $KClO_4$ was subsequently introduced to each soil column at constant flow rate with a peristaltic pump (BT 102S, Baoding Longer Precision Pump Co., Ltd., Hebei, China). It was followed by a leaching or desorption pulse consists of pumping the background solution. Effluent samples were collected from the outlet of the column by an automatic effluent fraction collector (CBS-A, Shanghai Huxi Analysis Instrument Factory Co., Ltd., Shanghai) at 1 h time interval and analyzed on HG-AFS. To independently obtain estimates of the hydrodynamic dispersion

coefficient (D), separate pulses of a conservative bromide (Br) tracer solution were applied to each column. The Br data were fitted to the nonreactive convection–dispersion equation (CDE) to calculate best-fit parameters for D using nonlinear least square optimization.

2.4. Multi-reaction transport model

The multi-reaction model (MRM) developed by Selim et al. (1989) is utilized for describing the kinetic sorption–desorption and transport of Sb(V) in the IOCS. The MRM assumes that a set of equilibrium sorption sites interacts instantaneously with Sb(V) in solution whereas a set of reversible kinetic sites are time-dependent in nature. It is described in the following formulations:

$$S_e = K_e \frac{\theta}{\rho} C^n \tag{1}$$

$$\frac{\partial S_k}{\partial t} = k_1 \frac{\theta}{\rho} C^n - k_2 S_k \tag{2}$$

Here S_e is the Sb(V) retained on equilibrium sites (μmol g^{-1}), S_k is the Sb(V) retained on kinetic type sites (μmol g^{-1}), C is the Sb(V) concentration in solution (μmol L^{-1}), n is the dimensionless reaction order reflecting the nonlinear nature of Sb(V) sorption, K_e is an equilibrium distribution coefficient, k_1 and k_2 (h^{-1}) are the forward and backward reaction rates associated with kinetic sites, respectively. θ is the soil water content ($cm^3\ cm^{-3}$), ρ is the soil bulk density (g cm^{-3}), and t is the reaction time (h). To simulate the reactive transport of Sb(V) through soils, the MRM sorption–desorption formulations are incorporated into the steady state convection–dispersion equation (CDE) in the form of (Selim et al., 1989):

$$\frac{\partial C}{\partial t} + \frac{\rho}{\theta}\frac{\partial S}{\partial t} = \frac{\partial}{\partial x}\left(D\frac{\partial C}{\partial x}\right) - v\frac{\partial C}{\partial x} \tag{3}$$

where x is distance (cm), D is hydrodynamic dispersion coefficient ($cm^2\ h^{-1}$), and v is pore water velocity (cm h^{-1}). The total amount of Sb(V) retention (S) is calculated as the summation of S_e in Eq. (1) and S_k in Eq. (2).

3. Results and discussion

3.1. Equilibrium sorption

Equilibrium isotherms describing the distribution of Sb(V) between aqueous (C) and sorbed phases (S) are presented in Fig. 1(left). The Freundlich equation $S = K_F C^N$ (K_F is the Freundlich distribution coefficient and N is the nonlinear reaction order) and the Langmuir equation $S = S_{max}\frac{K_L C}{1+K_L C}$ (S_{max} is sorption maximum and K_L is the Langmuir coefficient) are employed to describe equilibrium sorption isotherms (Kinniburgh, 1986). Best-fit parameters and goodness-of-fit values are summarized in Table 1 for three reaction pHs. Although both Freundlich and Langmuir equations give highly significant ($P < 0.01$) fits to the Sb(V) sorption isotherms, the Freundlich model has significantly better agreement with experimental data, as exhibited by the higher values of coefficients of determination (R^2) when compared to the Langmuir model.

The Sb(V) isotherms clearly exhibit nonlinear sorption behavior, which is characterized by low values of the nonlinear reaction order N for pH = 4.0 ($N = 0.25 \pm 0.03$), pH = 6.0 ($N = 0.36 \pm 0.04$), and pH = 7.5 ($N = 0.52 \pm 0.03$). Freundlich N is commonly considered as a measure of heterogeneity of surface sites having different sorption affinities (Kinniburgh, 1986; Ho et al., 2002). The increase of N with solution pH shows that protonation–deprotonation reaction has a dominant impact on the affinity and heterogeneity of Sb (V) binding sites on surface of iron oxides. The low N values also indicate the dependence of sorption capacity on Sb(V) concentration where sorption by the highest energy sites occurs preferentially at the lowest Sb(V) concentration. Furthermore, the distribution coefficient K_F decreased from 0.34 ± 0.04 at pH 4.0 to 0.040 ± 0.006 at pH 7.5. It is consistent with the significant decrease of Langmuir sorption maxima (S_{max}) from

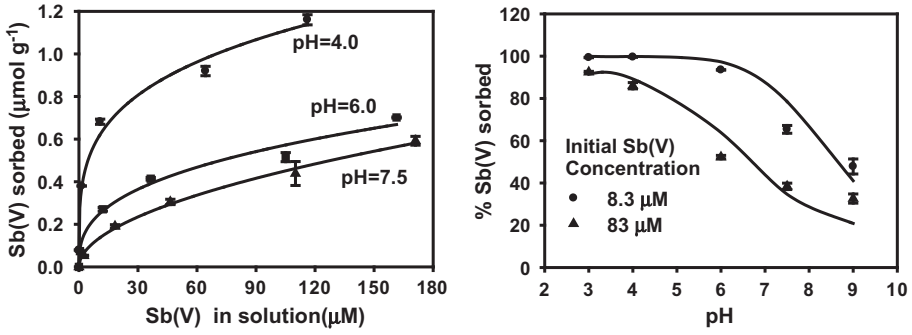

Fig. 1. Equilibrium sorption of Sb(V) on iron oxide coated sand (IOCS). Left: Sb(V) sorption isotherms with solid lines depict curve fitting of Freundlich equation. Right: Sb(V) sorption edges with solid lines depict surface complexation simulations. The experiments were performed by 48 h reaction of 3 g IOCS with 30 mL Sb(V) in 0.01 M $KClO_4$ at different solution pH and initial concentrations.

Table 1
Estimated Freundlich-and Langmuir-parameters (with standard error) for Sb(V) sorption on oxide coated sand (IOCS) at three pHs (4.0, 6.0, and 7.5).

pH	Langmuir			Freundlich		
	S_{max} (μmol kg^{-1})	K_L (L μmol^{-1})	R^2	K_F (L kg^{-1})	N	R^2
4.0	1.07 ± 0.09	3.9 ± 1.84	0.955	0.34 ± 0.04	0.25 ± 0.03	0.989
6.0	0.73 ± 0.09	25.0 ± 10.5	0.957	0.11 ± 0.02	0.36 ± 0.04	0.986
7.5	0.80 ± 0.10	71.9 ± 21.7	0.983	0.040 ± 0.006	0.52 ± 0.03	0.996

Table 2
Reaction constants used in surface complexation modeling of Sb(V) sorption on iron oxide coated sand (IOCS).

Reactions	log*K*	References
$Fe—OH + H^+ \leftrightarrow Fe—OH_2^+$	4.01	Vithanage et al. (2013)
$Fe—OH \leftrightarrow Fe—O^- + H^+$	−8.93	Vithanage et al. (2013)
$Sb(OH)_6^- + H^+ \leftrightarrow Sb(OH)_5 + H_2O$	2.85	Vithanage et al. (2013)
$\equiv Fe—OH + Sb(OH)_6^- + H^+ \leftrightarrow \equiv Fe—OH_2—Sb(OH)_6^-$	9.5	Optimized
$\equiv Fe—OH + Sb(OH)_6^- \leftrightarrow \equiv Fe—O—Sb(OH)_5^- + H_2O$	4.1	Optimized

1.07 ± 0.09 μmol kg^{-1} at pH 4.0 to 0.80 ± 0.10 μmol kg^{-1} at pH 7.5. Overall, the sorption isotherms illustrate that sorption of Sb(V) on IOCS is significantly higher and more nonlinear under acidic condition than under neutral to alkaline conditions.

To further illustrate the effect of protonation–deprotonation reaction on Sb(V) retention, sorption edges are shown in Fig. 1 (right) to describe Sb(V) sorption as a function of pH. At initial concentrations of 8.3 μM, Sb(V) sorption on IOCS decrease from 99.3% to 47.8% as pH increased from 3 to 9. This decrease of sorption capacity is consistent with previous studies on iron oxides (Essington, 2013; Guo et al., 2014) and red soils (Vithanage et al., 2013). Since antimonate is a moderately weak and monoprotic acid with a p*K*a of 2.85, the majority of Sb(V) is presented in the form of $Sb(OH)_6^-$ oxyanions in solution in the tested pH range (3–9) (Baes and Mesmer, 1986; Filella et al., 2002b; Hockmann and Schulin, 2012). As net surface charge of iron oxide change from positive to negative at higher pH, the increased electrostatic repulsion between antimonate anions and oxide surface might have resulted in the reduction of Sb(V) retention.

To describe the sorption edge data, surface complexation modeling is conducted using PhreeqC (Parkhurst and Appelo, 1999) with parameters optimized using general non-linear parameter estimation program (PEST) (Doherty, 2004). Previous spectroscopic studies indicate that Sb(V) might be retained on iron oxide surfaces by both specific and nonspecific adsorption through formation of inner-sphere or outer-sphere surface complexes (Leuz et al., 2006; Scheinost et al., 2006; Mitsunobu et al., 2010; Guo et al., 2014). Here we follow the model formation of Essington (2013) and assume Sb(V) is adsorbed on IOCS by formation of monodentate inner-sphere species [$\equiv Fe—O—Sb(OH)_5^-$] and outer-sphere species [$\equiv Fe—OH_2—Sb(OH)_6^-$]. The reaction constants used in the surface complexation model are given in Table 2 and the simulation results are plotted in Fig. 1(right). Overall, Sb(V) sorption is well-predicted by this model in the tested pH and concentration range. The optimized logarithm of intrinsic surface complexation constants (log*K*) are 9.5 for the outer-sphere complex and 4.1 for the inner-sphere species. The results showed that inner-sphere surface complex is the predominant surface species throughout the tested pH range. This is consistent with results from the spectroscopic studies (Mitsunobu et al., 2010; Guo et al., 2014) and surface complexation modeling studies on iron oxides (Vithanage et al., 2013; Essington, 2013).

3.2. Kinetic sorption–desorption

The results of kinetic batch experiments are presented in Fig. 2 to illustrate the changes in Sb(V) sorption versus time for two input concentrations at three different pHs. The results clearly demonstrate that Sb(V) sorption by IOCS is fast in the first two hours and followed a slow process that extend for days to weeks. This is consistent with previous studies which revealed that Sb (V) sorption was initially rapid (Ambe, 1987) followed by a slow retention rate (Leuz et al., 2006; Martinez-Llado et al., 2011; Zhang et al., 2014). A more interesting feature is that the sorption becomes slower as the reaction pH increases, especially at low surface coverage. Although multiple studies have demonstrated the decrease of sorption capacities with increasing pH on minerals (Leuz and Johnson, 2005; Tighe et al., 2005; Rakshit et al., 2015) and soils (Biver et al., 2011; Vithanage et al., 2013), we are not aware of any studies on the protonation–deprotonation reaction effect on the kinetic rate of Sb(V) sorption. The kinetic study of As(III and V) and silicic acid sorption on goethite conducted by Waltham and Eick (2002) showed that the adsorption rate was the greatest at pH values near their pK_1 values. Therefore, the affinity of antimonate (pK_1 = 2.85) for iron oxide surface should be the highest at acidic condition and decreases with increasing pH. A range of physical (diffusion limited) and chemical (reaction limited) mechanisms might contribute to the slow sorption of Sb(V) on iron oxides. The formation of surface precipitation is unlikely in the reaction system because Sb(V) concentrations are undersaturated with respect to Sb minerals and the available surface sites on IOCS are greater than the quantity of Sb(V). We cannot rule out the possibility of the change of types of surface complexes (mono- to bi-dentate) on the surface of iron oxides (Fendorf et al., 1997), further spectroscopic evidences will be required to verify the variation of Sb(V) surface structure with reaction time. But we believe that physical non-equilibrium, i.e., slow diffusion into interparticle and intraparticle pores or spaces, is the dominant

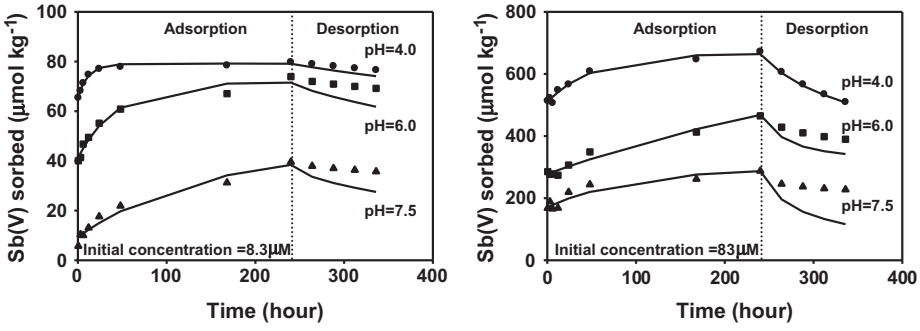

Fig. 2. Sorption–desorption kinetics of Sb(V) on iron oxide coated sand (IOCS) at three pHs (4.0, 6.0, and 7.5) and two initial concentrations (8.3 and 83 μM). The experiments were performed by mixing 3 g IOCS with 30 mL Sb(V) solution prepared in 0.01 M $KClO_4$. Lines are multi-reaction model (MRM) simulations using sorption parameters (K_e, k_1, and k_2) obtained from nonlinear optimization.

mechanism of observed slow retention of Sb(V) by IOCS. Furthermore, we propose that the diffusion of Sb(V) oxyanions with respect to electrostatic forces on variable charge surface (i.e., the Nernst–Planck electrodiffusion) can be used to explain the change of kinetic rate with pH. Specifically, increased electrostatic repulsion between iron oxide surface and aqueous oxyanions resulted in slower mass transfer of Sb(V) to IOCS under high solution pH.

As shown in Fig. 2, the total amount of Sb(V) released as a percentage of that sorbed are only 2–4% and 19–28% for the initial concentration of 8.3 μM and 83 μM, respectively. This is consistent with the sorption isotherms and surface complexation simulation, both demonstrate that Sb(V) is strongly sorbed on high energy sites. The results also show that percentage of desorption increases at high Sb(V) input concentrations where increasing amount of sorption are with lower binding affinities. This corroborated the highly nonlinear Sb(V) sorption behavior indicated by low values of the Freundlich N (Table 1). Earlier studies show that Sb(V) released more rapidly at higher pH from iron oxide (McComb et al., 2007) and kaolinite (Xi et al., 2010) as a result of low sorption affinity. But in our reaction, the desorption were performed by successive dilution with same background solution of 0.01 M $KClO_4$ and the reaction pH gradually approached equilibrium, which explains the relatively stable fraction of desorption with respect to initial solution pH.

Given the highly nonlinear and time-dependent nature of Sb(V) sorption on IOCS, the MRM model is employed to describe the kinetic sorption–desorption data. The formulation is a fully reversible equilibrium-kinetic MRM variation with 4 reaction parameters K_e, k_1, k_2, and n. The Freundlich N in Table 1 is used in place of n throughout our simulation based on the recommendation of Zhang and Selim (2005). Best-fit of other 3 kinetic rate parameters (i.e., K_e, k_1, and k_2) is obtained on the basis of the Levenberg–Marquardt nonlinear least-squares optimization method. The coefficients of determination (R^2) and the root-mean-square error (RMSE) are used as statistical criteria for estimating the goodness-of-fit. Comparison of parameters and goodness-of-fit from fitting kinetic MRM model to sorption–desorption data at different initial concentration (C_0) and pHs are given in Table 3.

Based on the goodness-of-fit in Table 3, the equilibrium-kinetic MRM successfully simulated the time-dependent sorption of Sb(V) on surface of IOCS with optimized parameters K_e, k_1, and k_2 but overpredicted Sb(V) desorption. It should be noted that the same set of optimized parameters applied for both adsorption and desorption processes. The departure of MRM simulation from observation during desorption process might be caused by pH variation in the desorption phase. A detailed examination show that all three model parameters decrease with a increase in pH, which clearly indicate the reduction of sorption capacity and rate as solution become more alkaline. In addition, the simulation result show that the fraction of equilibrium sorption phase (S_e) decrease while the kinetic sorption phase (S_k) increase with reaction time. At initial Sb(V) concentration of 8.3 μM, the fractions of kinetic sorption (S_k) over total sorption (S) are 49.3%, 71.2%, and 83.1% at pH 4.0. 6.0, and 7.5, respectively, which indicate that overall Sb(V) sorption become more kinetic as negative electrostatic potential accumulate on surface of iron oxide.

3.3. Non-equilibrium transport

Experimental breakthrough curves (BTCs) are presented in Fig. 3 to describe the miscible displacement of Sb(V) in IOCS columns with solution pH at 4.0, 6.0, and 7.5. Measured Sb(V) BTCs exhibited extensive asymmetry as illustrated by the difference between the shape of the effluent side on the left and the leaching or desorption side on the right. The BTCs show a fast breakthrough to C/C_0 of 0.7–0.8 followed by gradual increase to full breakthrough ($C/C_0 = 1$). A sharp decrease of Sb(V) concentration can be observed once the input solution [0.15 mM Sb(V)] is replaced by background solution of 0.01 M $KClO_4$. An extended slow release of Sb(V) at relatively low concentration can extend another 100–200 pore volumes until the effluent concentration is below detection limit. Similar asymmetric BTCs for Sb(V) has been observed by Martinez-Llado et al. (2011) from column experiments conducted on calcareous soils with reaction pH of 7.0–7.8. However, the BTCs are contrastingly different from that of Zhang et al. (2014), where a much longer retardation and lower peak concentration ($C/C_0 < 0.12$ for acidic red soil and $C/C_0 < 0.55$ for calcareous soils) was observed. The difference between the BTCs can be explained by the dissimilar contents of iron and aluminum oxides in column media. The iron oxide content of IOCS used in our experiment falls in the range of that in columns of Martinez-Llado et al. (2011) but an order of magnitude lower than the two natural soils used in the experiment of Zhang et al. (2014).

More importantly, arrival time of the breakthrough front and mass recovery of BTCs vary significantly with reaction pH. It takes approximately 70, 8, and 3 pore volumes for Sb(V) to breakthrough at pH 4.0, 6.0, and 7.5, respectively. The Sb(V) mass recovery (percentage of amount in column effluent over total amount of solute input) increased from 70.3% at pH 4.0 to 87.5% at pH 6.0 and further increased to 91.6% at pH 7.5. This increase of Sb(V) mobility with the increasing pH is consistent with the results of batch experiment, where sorption substantially declined as the reaction system become more alkaline. In addition, the extended gradual increase of C/C_0 to full breakthrough is a sign of the non-equilibrium or time-dependent retention of Sb(V), which is also shown in the kinetic sorption experiment. Furthermore, a substantial fraction of applied Sb(V) remains in soil column even after extended leaching with Sb free background solution for some 200 pore volumes. It is expected because the kinetic sorption experiment demonstrate that Sb(V) is strongly retained on surface of iron oxide and only a small fraction of sorbed Sb(V) can be desorbed, especially at low pH when the sorption was the strongest. Overall, the miscible displacement experiment elucidates that the transport of Sb(V) in IOCS columns is dominated by non-equilibrium retention on surface of iron oxides and the protonation–deprotonation reaction has a major impact on the mobility of Sb(V).

To describe the non-equilibrium Sb(V) transport through IOCS columns, the MRM model was utilized in two different mode, i.e., a predictive mode and an optimized mode. The simulated BTCs are illustrated in Fig. 3 to compare with the measured BTCs. In both simulation modes, the hydrodynamic dispersion coefficient ($D = 5 \times 10^{-5}$ m^2 h^{-1}) in Eq. (3) is obtained from fitting the non-reactive CDE to BTCs of bromide (Br), which used as a conservative tracer. In addition, other transport parameters such as pore water velocity ($v = 0.04$ m h^{-1}), bulk density ($\rho = 1.60$ Mg m^{-3}), moisture content ($\theta = 0.4$ m^3 m^{-3}), and applied concentration ($C_0 = 0.15$ mM) are based on actual measurements. In the predictive mode, all necessary model parameters are obtained independently from the experiment BTCs being modeled. The sorption–desorption parameters (K_e, k_1, k_2, and n) from the fitting the kinetic batch data are used to simulated the retention on equilibrium (S_e) and kinetic (S_k) phases. Consistent with previous studies (Zhang et al., 2014), using kinetic batch rate coefficients overpredicted Sb(V) concentration peaks and underestimated the extent of retardation for all three reaction pHs.

In the optimized mode, inverse modeling is conducted by optimizing the kinetic parameters (K_e, k_1, and k_2) through fitting the MRM model of Eqs. (1)–(3) to observed BTCs. The Levenberg–Marquardt nonlinear least-squares optimization method is utilized and the goodness-of-fit is evaluated using R^2 and RMSE. Table 3

Table 3
Comparison of sorption parameters (K_e, k_1, and k_2) and goodness-of-fit from fitting kinetic MRM model to kinetic batch data and column transport at different initial concentration (C_0) and pH values.

Experiments	C_0 (μM)	pH	R^2	RMSE	K_E	k_1 (h^{-1})	k_2 (h^{-1})
Batch	8.3	4	0.982	0.121	55.7 ± 1.0	0.22 ± 0.02	0.031 ± 0.005
	8.3	6	0.985	0.338	24.4 ± 1.0	0.062 ± 0.008	0.008 ± 0.002
	8.3	7.5	0.997	0.330	3.2 ± 0.4	0.011 ± 0.002	0.004 ± 0.002
	83	4	0.994	1.817	212 ± 4.0	0.21 ± 0.03	0.012 ± 0.002
	83	6	0.994	3.640	65.2 ± 3.0	0.034 ± 0.011	0.004 ± 0.003
	83	7.5	0.996	3.302	19.2 ± 1.4	0.020 ± 0.008	0.007 ± 0.005
Column	150	4.0	0.931	18.68	56.8 ± 50	29.7 ± 6.0	0.013 ± 0.003
	150	6.0	0.987	9.48	21.4 ± 1.8	4.4 ± 0.5	0.006 ± 0.001
	150	7.5	0.979	12.51	0.8 ± 209	1.3 ± 1.1	0.005 ± 0.002

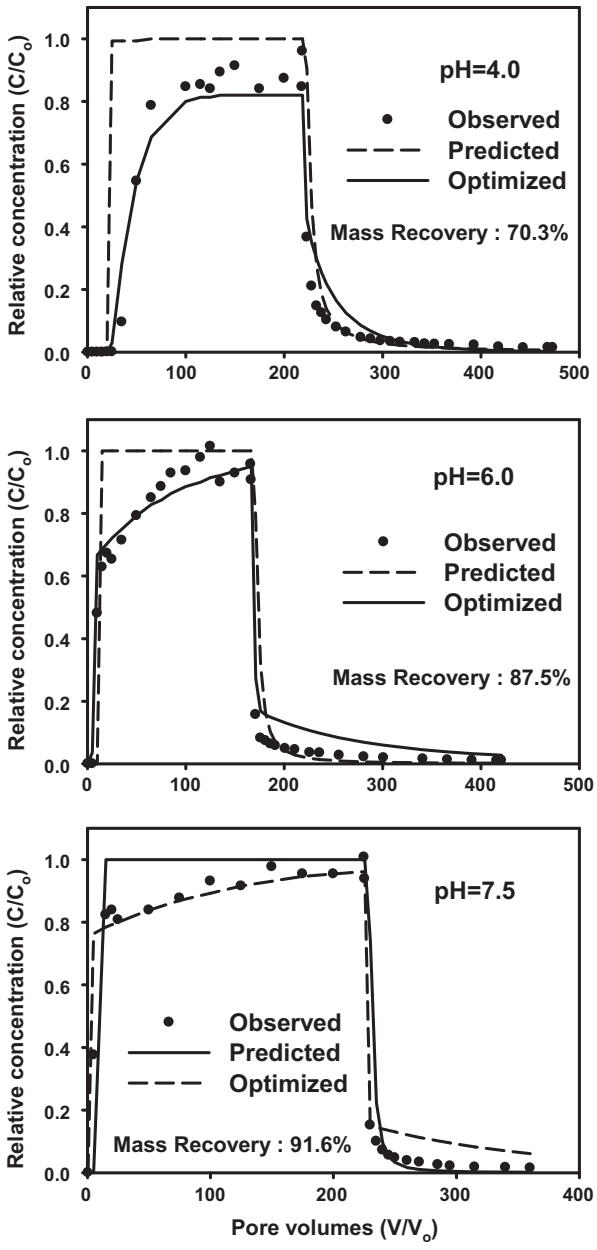

Fig. 3. Breakthrough curves (BTCs) of Sb(V) from columns of iron oxide coated sand (IOCS) at three pHs (4.0, 6.0, and 7.5). The symbols are experiment observations with initial Sb(V) concentration of 0.15 mM and pore water velocity (v) of 0.04 m h^{-1}. Dashed and solid lines are MRM simulations using sorption parameters (K_e, k_1, and k_2) from kinetic batch experiments and nonlinear optimization, respectively.

gives the optimized MRM parameters and goodness-of-fit for BTCs at different reaction pHs. Excellent fits of the MRM model are achieved for all Sb(V) BTCs as indicated by values of RMSE and R^2. Sorption rate coefficients (k_1) obtained from column BTCs are two orders of magnitude larger than those from kinetic sorption–desorption data (Table 3), which is indicative of stronger kinetic sorption in columns than in batch reactors. The equilibrium distribution coefficients (K_e) and desorption rate coefficients (k_2) behave comparably similar between the column and batch reactors. It suggests that the higher sorption might be caused by different sorption duration as a result of hydrologic residence time in miscible displacement experiments. Other factors such as low soil/solution ratio and increased spatial heterogeneity of sorption sites might also contribute to the observed discrepancy between reaction systems (Zhang and Selim, 2006). Similar to kinetic sorption simulation, all three MRM rate coefficients (K_e, k_1, and k_2) decrease with an increase in solution pH, reflecting decreased retention (increased mobility) of Sb(V) as the solution become neutral to alkaline.

In general, transport of antimony in vadose zone and aquifer can be controlled by a range of physical (Darcy flow, pore network, preferential flow, colloid facilitated transport, etc.) and geochemical factors (solute concentration, iron and aluminum oxides, organic material, pH, ionic strength, competing anions, redox condition, etc.). Accurate simulation of Sb movement should be based on thorough understanding of the individual and compounded effects of the controlling factors. In this study, we demonstrate the complex interaction between solution pH and retention kinetics in Sb(V) reaction and transport based on the results from laboratory experiments and numerical simulations. An important implication is that not only Sb(V) sorption capacity but also kinetics rates of sorption can be impacted by reaction pH. The non-equilibrium or time-dependent transport could result in slow release of Sb(V) for extended period of time, which need to be considered in environmental risk assessment and remediation design at Sb contaminated sites. The nonlinear MRM with equilibrium and kinetic sorption sites was capable of describing time-dependent retention and transport of Sb(V) using optimized parameters. However, this model has limitations since it does not directly consider pH as a model parameter. Incorporating surface complexation mechanisms into kinetic retention model will likely to result a more generic model with better capability to handle geochemical variables in transport modeling and should be further explored.

4. Conclusions

The kinetic batch and miscible displacement experiments results exhibit that an increase of solution pH causes decreasing sorption capacity and increasing mobility of Sb(V) in iron oxide

coated sand. The sorption isotherms illustrate that Sb(V) sorption on IOCS become significantly stronger and more nonlinear under acidic condition. As indicated by surface complexation modeling, formation of inner-sphere surface complex on surface of iron oxide is the predominant mechanisms and can explain the pH-dependency of Sb(V) sorption. The kinetic sorption results clearly demonstrate that Sb(V) sorption by IOCS is a time-dependent process where the reaction was fast in the first two hours and followed a slow process that extend for weeks. The sorption rate is the highest at acidic condition and decrease with increasing pH due to the low dissociation constant of antimonate ($pK_1 = 2.85$). The miscible displacement experiment result show that Sb(V) transport is dominated by non-equilibrium retention on surfaces of iron oxides.

The fully reversible equilibrium-kinetic MRM successfully simulated the time-dependent sorption of Sb(V) on surface of IOCS with three optimized parameters (K_e, k_1, and k_2). The kinetic rates decrease with increasing pH, which clearly indicate the reduction of sorption capacity and rate as solution become more alkaline. The BTCs simulated using kinetic batch rate coefficients overpredicted Sb(V) mobility and underestimated the extent of retention for all three reaction pHs. Inverse modeling conducted by optimizing the MRM parameters (K_e, k_1, and k_2) provides excellent fits for all Sb(V) BTCs and the optimized forward rate coefficients (k_1) are two orders of magnitude larger than those from kinetic batch data (Table 3), indicating stronger kinetic sorption in columns than in batch reactors. Although our modeling effort could reveal the complex interaction between solution pH and retention kinetics in Sb (V) transport, further modeling efforts (possibly by incorporating the surface complexation mechanisms into the kinetic retention and transport models) is required to simulate the fate and behavior of Sb(V) under dynamic geochemical conditions.

Acknowledgments

The authors would like to thank Dr. Xueli Wu for chemical analysis. This work was financially supported by the National Natural Science Foundation of China (41271506, 41230858) and Key Research Program of the Chinese Academy of Sciences (KZZD-EW-14). Dr. Hua Zhang was financially supported by the Recruitment Program of Global Young Experts (1000Plan).

References

Accornero, M., Marini, L., Lelli, M., 2008. The dissociation constant of antimonic acid at 10–40 °C. J. Solution Chem. 37, 785–800.
Ambe, S., 1987. Adsorption kinetics of antimony (V) ions onto alpha-Fe_2O_3 surfaces from an aqueous solution. Langmuir 3, 489–493.
Baes, C.F., Mesmer, R.E., 1986. The Hydrolysis of Cations. Krieger, Malabar, FL.
Beyersmann, D., Hartwig, A., 2008. Carcinogenic metal compounds: recent insight into molecular and cellular mechanisms. Arch. Toxicol. 82, 493–512.
Biver, M., Krachler, M., Shotyk, W., 2011. The desorption of antimony (V) from sediments, hydrous oxides, and clay minerals by carbonate, phosphate, sulfate, nitrate, and chloride. J. Environ. Qual. 40, 1143–1152.
Doherty, J., 2004. PEST, Model Independent Parameter Estimation User Manual, fifth ed. Watermark Numerical Computing, Berlin.
Essington, M.E., 2013. Antimony (V) Adsorption by Variable-Charge Minerals. Strategic Environmental Research and Development Program (SERDP) Project ER-1741 Report. USDOD, Washington, D.C.
Fendorf, S., Eick, M.J., Grossl, P., Sparks, D.L., 1997. Arsenate and chromate retention mechanisms on goethite. 1. Surface structure. Environ. Sci. Technol. 31, 315–320.
Filella, M., Belzile, N., Chen, Y.W., 2002a. Antimony in the environment: a review focused on natural waters I. Occurrence. Earth-Sci. Rev. 57, 125–176.
Filella, M., Belzile, N., Chen, Y.W., 2002b. Antimony in the environment: a review focused on natural waters: II. Relevant solution chemistry. Earth-Sci. Rev. 59, 265–285.
Frohne et al., 2011. Controlled variation of redox conditions in a floodplain soil: impact on metal mobilization and biomethylation of arsenic and antimony. Geoderma 160, 414–424.
Gebel, T., Christensen, S., Dunkelberg, H., 1997. Comparative and environmental genotoxicity of antimony and arsenic. Anticancer Res. 17, 2603–2608.
Guo, X., Wu, Z., He, M., Meng, X., Jin, X., Qiu, N., Zhang, J., 2014. Adsorption of antimony onto iron oxyhydroxides: adsorption behavior and surface structure. J. Hazard. Mater. 276, 339–345.
He, M.C., Wang, X.Q., Wu, F.C., Fu, Z.Y., 2012. Antimony pollution in China. Sci. Total Environ. 421–422, 41–50.
Ho, Y.S., Porter, J.F., Mckay, G., 2002. Equilibrium isotherm studies for the sorption of divalent metal ions on to peat: copper, Nickel and Lead single component systems. Water Air Soil Pollut. 141, 1–33.
Hockmann, K., Schulin, R., 2012. Leaching of antimony from contaminated soils. In: Selim, H.M. (Ed.), Competitive Sorption and Transport of Heavy Metals in Soils and Geological Media. CRC Press, Boca Raton, FL, pp. 119–145.
Hockmann, K., Lenz, M., Tandy, S., Nachtegaal, M., Janousch, M., Schulin, R., 2014. Release of antimony from contaminated soil induced by redox changes. J. Hazard. Mater. 275, 215–221.
Ilgen, A.G., Trainor, T.P., 2012. Sb (III) and Sb (V) sorption onto Al-rich phases: hydrous Al oxide and the clay minerals kaolinite KGa-1b and oxidized and reduced nontranite NAu-1. Environ. Sci. Technol. 46, 843–851.
Ilgen, A.G., Majs, F., Barker, A.J., Douglas, T.A., Trainor, T.P., 2014. Oxidation and mobilization of metallic antimony in aqueous systems with simulated groundwater. Geochim. Cosmochim. Acta 132, 16–30.
Kinniburgh, D.G., 1986. General purpose adsorption isotherms. Environ. Sci. Technol. 20, 895–904.
Leuz, A.K., Johnson, C.A., 2005. Oxidation of Sb (III) to Sb (V) by O_2 and H_2O_2 in aqueous solutions. Geochim. Cosmochim. Acta 69, 1165–1172.
Leuz, A.K., Monch, H., Johnson, C.A., 2006. Sorption of Sb (III) and Sb (V) to goethite: influence on Sb (III) oxidation and mobilization. Environ. Sci. Technol. 40, 7277–7282.
Martinez-Llado, X., Valderrama, C., Rovira, M., Marti, V., Gimenez, J., de Pablo, J., 2011. Sorption and mobility of Sb (V) in calcareous soils of Catalonia (NE Spain): batch and column experiments. Geoderma 160, 468–476.
McComb, K.A., Craw, D., McQuillan, A.J., 2007. ATR-IR spectroscopic study of antimonate adsorption to iron oxide. Langmuir 23, 12125–12130.
Mitsunobu, S., Takahashi, Y., Terada, Y., Sakai, M., 2010. Antimony (V) incorporation into synthetic ferrihydrite, goethite, and natural iron oxyhydroxides. Environ. Sci. Technol. 44, 3712–3718.
Parkhurst, D.L., Appelo, C.A.J., 1999. User's guide to PHREEQC Version 2-A Computer Program for Speciation, Batch Reaction, One-Dimensional Transport and Inverse Geochemical Calculations. Water Resources Investigations. Report 99–4259. U. S. Geological Survey, Lakewood CO.
Rakshit, S., Sarkar, D., Datta, R., 2015. Surface complexation of antimony on kaolinite. Chemosphere 119, 349–354.
Ritchie, V., Ilgen, A.G., Mueller, S.H., Trainor, T.P., Goldfarb, R.J., 2013. Mobility and chemical fate of antimony and arsenic in historic mining environments of the Kantishna Hills district, Denali National Park and Preserve, Alaska. Chem. Geol. 335, 172–188.
Scheinost, A.C., Rossberg, A., Vantelon, D., Xifra, I.O., Kretzschmar, R., Leuz, A.K., Funke, H., Johnson, C.A., 2006. Quantiative antimony speciation in shooting-range soils by EXAFS spectroscopy. Geochim. Cosmochim. Acta 70, 3299–3312.
Selim, H.M., Amacher, M.C., Iskandar, I.K., 1989. Modeling the transport of chromium (VI) in soil columns. Soil Sci. Soc. Am. J. 53, 996–1004.
Takayanagi, K., Cossa, D., 1997. Vertical distributions of Sb (III) and Sb (V) in Pavin Lake, France. Water Res. 31, 671–674.
Tighe, M., Lockwood, P., 2007. The importance of non-crystalline hydroxide phases in sequential extractions to fractionate antimony in acid soils. Commun. Soil Sci. Plant Anal. 38, 1487–1501.
Tighe, M., Lockwood, P., Wilson, S., 2005. Adsorption of antimony (V) by floodplain soils, amorphous iron (III) hydroxide and humic acid. J. Environ. Monitor. 7, 1177–1185.
Vithanage, M., Rajapaksha, A.U., Dou, X.M., Bolan, N.S., Yang, J.E., Ok, Y.S., 2013. Surface complexation modeling and spectroscopic evidence of antimony adsorption on iron-oxide-rich red earth soils. J. Colloid Interface Sci. 406, 217–224.
Waltham, C.A., Eick, M.J., 2002. Kinetics of arsenic adsorption on goethite in the presence of sorbed silicic acid. Soil Sci. Soc. Am. J. 66, 818–825.
Wang, D.J., Bradford, S.A., Harvey, R.W., Gao, B., Cang, L., Zhou, D.M., 2012. Humic acid facilitates the transport of ARS-labeled hydroxyapatite nanoparticles in iron oxyhydroxide-coated sand. Environ. Sci. Technol. 46, 2738–2745.
Wang, D.J., Bradford, S.A., Paradelo, M., Peijnenburg, W.J.G.M., Chu, L.Y., Zhou, D.M., 2011. Facilitated transport of copper with hydroxyapatite nanoparticles in saturated sand. Soil Sci. Soc. Am. J. 76, 375–388.
Willis, S.S., Haque, S.E., Johannesson, K.H., 2011. Arsenic and antimony in groundwater flow systems: a comparative study. Aquat. Geochem. 17, 775–807.
Wilson, S.C., Lockwood, P.V., Ashley, P.M., Tighe, M., 2010. The chemistry and behaviour of antimony in the soil environment with comparisons to arsenic: a critical review. Environ. Pollut. 158, 1169–1181.
Xi, J., He, M.C., Lin, C.Y., 2010. Adsorption of antimony (V) on kaolinite as a function of pH, ionic strength and humic acid. Environ. Earth Sci. 60, 715–722.
Zhang, H., Li, L.L., Zhou, S.W., 2014. Kinetic modeling of antimony (V) adsorption–desorption and transport in soils. Chemosphere 111, 434–440.
Zhang, H., Selim, H.M., 2005. Kinetics of arsenate adsorption–desorption in soils. Environ. Sci. Technol. 39, 6101–6108.
Zhang, H., Selim, H.M., 2006. Modeling the transport and retention of arsenic (V) in soils. Soil Sci. Soc. Am. J. 70, 1677–1687.
Zhang, H., Selim, H.M., 2011. Second-order modeling of arsenite transport in soils. J. Contam. Hydrol. 126, 121–129.